Estimate of river seepage by conditioning downward groundwater flow in the Toyohira River alluvial fan, Japan

Yoshitaka Sakata [a], Gur Baran [b], Teruhiko Suzuki [b] and Kazuhisa A Chikita [c]

[a]*Environmental System Research Laboratory, Division of Human Environmental Systems, Faculty of Engineering, Hokkaido University, Sapporo, Japan*

y-sakata@eng.hokudai.ac.jp

[b]*GM Labo Ltd, Sapporo, Japan*

[c]*Department of Natural History Sciences, Faculty of Science, Hokkaido University, Sapporo, Japan*

Corresponding author:

Yoshitaka Sakata

Postal address: North-13, West-8, Kita-ku, Sapporo, Hokkaido 060-0828, Japan

E-mail: yoshitaka_sakata@mail.sci.hokudai.ac.jp

Telephone: +81-11-706-6288

Contributing authors:

Gur Baran

Postal address: Oyachi-Higashi-3, Atsubetsu-ku, Sapporo, Hokkaido 004-0041, Japan

E-mail: baran@gmlabo.co.jp

Telephone: +81-11-777-2588

Teruhiko Suzuki

Postal address: Oyachi-Higashi-3, Atsubetsu-ku, Sapporo, Hokkaido 004-0041, Japan

E-mail: suzuki@gmlabo.co.jp

Telephone: +81-11-777-2588

Kazuhisa A Chikita

Postal address: North-10, West-8, Kita-ku, Sapporo, Hokkaido 060-0810, Japan

E-mail: chikita@mail.sci.hokudai.ac.jp

Telephone: +81-11-706-2764

Estimate of river seepage by conditioning downward groundwater flow in the Toyohira River alluvial fan, Japan

River seepage serves as the main source of groundwater in alluvial fans. However, reasonable estimates are rarely obtainable due to inaccuracy of vertical flows around the losing river. In the alluvial fan of the Toyohira River, Japan, to provide straightforward description of vertical hydraulic gradient, this study demonstrates to assign constant head boundary conditions on the shallowest aquitard instead of no flow conditions on the basement. Initial constant heads and layer-scale anisotropy are calibrated in terms of hydraulic heads. As a result, the simulated river seepage is in reasonable agreement with previous discharge measurements, with net water loss determined to be approximately 1 m^3/s. Although the simulation fails water gain in the lower section, due to a lack of sporadic intercalations of fine deposits, the conditioned vertical hydraulic gradient modeling approach is found to be effective on a regional scale, especially when losing/gaining sections have not been identified in advance.

Keywords: Groundwater, River seepage, Numerical simulation, Aquifer modeling, Water budget, Alluvial fan

INTRODUCTION

Alluvial fans serve as water reservoirs that contribute to industry, agriculture, and urbanization around the world. This natural water storage is valuable, especially in arid and semi-arid regions, where an aggradation of coarse deposits promotes fan development under sparse vegetation and intense rainfall. Despite Japan's humid climate, there are 314 alluvial fans around the feet of mountains, a result of tectonic activity and sea-level changes in the last glacial period (Ono 1990, pp. 91–108). In general, fans are limited in extent; most alluvial fans in Japan have areas of more than 2 km^2 but less than 100 km^2 (Saito 1998, pp. 257–266). In addition, gravelly aquifers are susceptible to excessive withdrawal, such that land subsidence and water pollution

occur rapidly and widely over alluvial fans (e.g., Fetter 2001, pp. 325–327, Jang *et al*. 2005, Chen *et al*. 2010, Maruyama *et al*. 2013). Recent studies also suggest that climate change might significantly influence groundwater vulnerability in alluvial fans (Hu *et al*. 2010a). River seepage is the primary source of groundwater in alluvial fans (Bull 1964, Houston 2002, Blainey and Pelletier 2008). Surface water infiltrates through highly permeable gravel beds according to high river stages relative to the groundwater table. While important for groundwater vulnerability, river seepage might be problematic in terms of surface water use and ecological conservation, especially during drought periods (Sophocleous 2002). Therefore, quantifying river seepage is imperative in an alluvial fan for efficient management of both groundwater and surface water.

Numerical simulation of groundwater flow is traditionally used to provide estimates of hydraulic heads and determine the exchange between surface water and groundwater (e.g., Fugazza *et al*. 1983, Pucci and Pope 1995, Nobi and Gupta 1997, Rodríguez *et al*. 2006, Pisinaras *et al*. 2007). Various field methods (e.g., discharge measurement, seepage meters, and geochemical and physical tracers) can provide more direct estimates in local area (Weight 2008, pp. 231–286). However, these measurements are restricted with respect to space and time; consequently, these methods might be effective only when the losing and gaining sections have been approximately identified in advance. When estimating river seepage is required on a regional scale (e.g., over an alluvial fan), a numerical modeling approach is more flexible and inexpensive at various scales and under various simulation scenarios (Gupta and Onta 1997).

Water exchange between surface water and groundwater is estimated according to Darcy's law, which is a combination of the hydraulic gradient between stream stage and groundwater head with streambed conductance that accounts for streambed

thickness, hydraulic conductivity, and streambed areas (Anderson and Woessner 1992, pp. 160–163, Healy 2010, pp. 57–60). Recent high-resolution models focus on the heterogeneity of streambed conductance (e.g., Fleckenstein *et al*. 2006, Sebok *et al*. 2014). However, streambed conductivity may not necessarily be critical when the values are comparatively high and the target is regional water resources (Calver 2002). In other words, a description of hydraulic gradients around the river is also important for estimating river seepage on a regional scale, especially in alluvial fans where gravelly streambeds have relatively high permeability.

Hydraulic gradients are three dimensional around losing rivers and streams as a result of water exchange between groundwater and surface water. Surface water that infiltrates gravelly streambeds moves laterally near the water table and vertically into deeper layers. Especially in gravel-bed rivers with low flow, the water depth is much smaller than the river width, and the seepage area is occupied by the streambed. In other words, the seepage fluxes are dominant in the vertical direction, and the infiltrated water moves laterally in the shallow layer and vertically into the deep layer. Because alluvial fans consist of monotonic gravel sequences with relatively large thicknesses and permeability, river seepage might be controlled by the vertical hydraulic gradients, not only around the river but also throughout the deeper extents. However, it is common that uncertainty in groundwater flow simulation increases with depth due to a lack of geologic and head data. Also, in alluvial fans, impermeable basements (e.g., consolidated rocks) suddenly decline downstream to a depth of several hundreds or thousands of meters. Most regional models are constructed to such deep hydrologic basements, as suggested in many texts (e.g., Anderson and Woessner 1992, pp. 28–29). However, these results are not necessarily accurate with respect to hydraulic gradients

in the subsurface around the river channel, necessary for quantitatively estimating river seepage.

This study examines a straightforward modeling approach that considers downward groundwater flow around a losing river, using as a case study the Toyohira River alluvial fan in Sapporo, Japan. The vertical hydraulic gradient shows a negative peak along the river, indicating downward flow fluxes as a result of excessive pumping in a deeper layer of the fan. A numerical groundwater model is constructed by specifying constant boundary conditions on the shallowest aquitard, instead of no flow conditions on the impermeable basements, by incorporating two maps, one of vertical hydraulic gradient (VHG) and one of water table elevation (WTE). The initial VHG is adjusted, and layer-scale anisotropy is assumed to obtain a match between simulated and observed heads. Water exchange in each river cell is summed from the upper point (the confluence with the main tributary), and the surface water budget reasonably agrees with the results of a previous synoptic discharge survey. River seepage in the fan is estimated and the effectiveness and limitations of this modeling approach are assessed.

MATERIALS AND METHODS

Study site

The field site is the Toyohira River alluvial fan in Sapporo (near 43°N 141°E) on Hokkaido, the northernmost island of Japan (Fig. 1). Sapporo is the most urbanized city in northern Japan, with a population of over 1.9 million people and rising. The Toyohira River, one of the tributaries of the Ishikari River, is approximately 72.5 km long with a watershed area of approximately 900 km^2. The river flows northward through the heart of Sapporo with a slope of 1/150 to 1/300, and the slope reduces to 1/1000 in the lowland out of the fan. From 1974−2011, median values of daily mean

discharges and drought discharges were 12.6 and 4.0 m^3/s, respectively. In particular, the flow rate suddenly increases at KP 18.5 due to a tributary, the Yamahana River, which contributes drainage from a hydraulic energy plant to the Toyohira River. Here, KP denotes distance in kilometers along the channel upstream from the confluence between the Toyohira River and the Ishikari River. The Toyohira River alluvial fan has a radius of approximately 7 km and covers an area of approximately 35 km^2. The fan is complex, consisting of a Holocene fan to the west and a Pleistocene fan to the east. These fans are topographically divided by the current river channel in the upper fan from approximately KP 15. The Holocene fan forms the main unconfined aquifer in the fan and the water table is mounded along the river, indicating interaction between surface water and groundwater, as shown later. In this study, a numerical model is constructed mainly of the Holocene fan because infiltrated water moves to the Holocene fan according to the relatively high permeability of the Holocene deposits (Hu *et al*. 2010b). For several decades, river seepage in the fan has been problematic for planning surface water use, especially in drought periods. In a previous study (Sakata and Ikeda 2012) we performed a synoptic river discharge survey of the river and determined that the leakage was approximately 1 m^3/s between KP 15.5 and KP 17. However, the previous study indicated that measurement errors of turbulent and unsteady flows might have contributed to inaccurate results. Thus, the current study investigates a numerical modeling approach and compares the results for river seepage in the fan with previous results.

Conceptual model

Figure 2 shows a longitudinal geologic cross section of the fan. This figure is modified from that in a previous study (Sakata and Ikeda 2013a). Tertiary volcanic formations form the fan basement, and suddenly incline northward due to tectonic

activity. Quaternary sediments overlie the basement and have a thickness of several hundreds of meters, and there are upward coarsening trends associated with changes in the depositional environment. As a result of sea level changes in the last glacial period, the lower strata consists of alternating layers of various sediments such as gravels, sand, silts, clays, and humus. At –50 to –30 m amsl, the sedimentary textures suddenly change to monotonic gravel sequences with thin fine layers. The boundary is distinguished as a muddy layer, which serves as the shallowest aquitard in the fan. The alluvial fan gravel deposits have a thickness of about 50 m on average, and of over 100 m at maximum. Median grain size of the bed materials gradually decreases exponentially in the downstream direction (Fig. 3). The decreasing slope is suddenly large at KP11, which corresponds to the end of the alluvial fan. Sakata and Ikeda (2013b) analyzed undisturbed gravel cores and determined that the gravel deposits are divided into shallow parts with an exponentially decreasing trend of permeability and deep parts with a stationary trend, as shown at OW18 and 20 in Fig. 2. Finer materials cover the ground in the lower fan and frequently intersect in the gravel deposits as a result of fan recession in the late Holocene. Consequently, formation of the fan is conceptually classified into four layers: alternating layers of coarse and fine sediments (Layer 4), deeper gravel deposits (Layer 3), shallower gravel deposits (Layer 2), and finer materials in the lower fan (Layer 1).

Water table and head contours in Figure 2 also show three dimensional system of groundwater flow in the subsurface of the fan. As in most alluvial fans, groundwater recharge occurs by surface water infiltration from the river, especially during drought periods. Infiltrated water flows mainly in the shallow Layer 2 due to its relatively high permeability. Some groundwater infiltrates the deeper Layers 3 and 4. In particular, the infiltration into Layer 4 is limited to only the upper fan, where the shallowest aquitard is

not continuously distributed. This also means that most of groundwater flows in Layers 2 and 3 between the middle and the lower fan. In the lower part (KP< 12), the vertical components of groundwater flow change from downward to upward flows, because the less permeable Layer 1 prevents lateral flow outside the fan.

Head contour maps

The Hokkaido Regional Development Bureau and the Geological Survey of Hokkaido have monitored groundwater levels at various locations. The first observation well was installed more than fifty years ago. Several observation sites include multiple wells with shallow and deep screen depths, that is, piezometer nests (shown as double circles in Fig. 1). The piezometer nests provide accurate VHG values at each location. In addition, to supplement the piezometer data, we observed groundwater levels at other individual wells on 20–21 October 2008. At the same time, the longitudinal river stage was measured for fixed heads on river cells. When compared with data for the past thirty years, it is evident that 2008 was a typical drought year (Japan Meteorological Agency 2012). Figure 4 shows daily variations of water levels in surface water and groundwater at piezometers for one month before the observation dates. R1 and R2 are gauging stations of river stages. OW4D (OW4S), OW17D (OW17S), and OW22D (OW22S) are deep (shallow) wells at the fan distal, middle, and apex areas. Details of these observations, such as screen depths, are available in Sakata and Ikeda (2013a). All observed water levels were almost consistent with amplitudes less than 0.1 m during one month, despite a total of 11 precipitation events. The largest precipitation was 25 mm/d on 9 October 2008. However, the consistent water level means that precipitation was negligible during the drought period. Therefore, the groundwater simulation reported herein was performed using drought head data under a steady condition where groundwater heads are balanced by only focused recharge from the river.

Figures 5a and 5b respectively show water table (WTE) and vertical hydraulic gradient (VHG) contour maps for the fan. These maps were drawn manually from October 2008 observation data and show almost the same features of the groundwater flow system as maps presented in the authors' previous publication (Sakata and Ikeda 2013a). The WTE contours (Fig. 5a) decline gently downstream (northward), but rise sharply along the river between KP 14 and KP 19, indicating that river stage is higher than water table around the river section. Depth to the water table increases as distance to the river increases: the depth is within several meters near the channel reach, and no more than 20 m in the center of the fan. The WTE mound induces surface water infiltration into the aquifer. Negative VHG contours (Fig. 5b) are accumulated around almost the same section as the WTE mound. Negative VHG values indicate downward flux of groundwater as a result of water infiltration from the river by pumping in the deeper layer, as well as by extensive underground construction such as subway lines. The VHG around the losing river has order of magnitude 10^{-1}, much higher than the WTE slopes, which have orders of magnitude 10^{-3} to 10^{-2}. If only the hydraulic gradient (except for the decaying trend of permeability with depth) is considered, groundwater around the losing river might flow more forcibly vertically than horizontally.

Numerical groundwater flow model

A three-dimensional finite-element model of groundwater flow in the fan was constructed (Fig. 6). The groundwater level in each cell was calculated by the finite element code AC-UNSAF3D, which was developed at Okayama University (1994). The model extends south to the southern mountainous and hilly area, east and west until the WTE mound (an effect of river seepage) is not evident, and north to a topographic boundary with the lowland (KP 11). The model surface is interpolated from a 50-m mesh digital elevation map of the Geological Survey Institute, Japan. However, for

increased accuracy, the surface around the river is modeled from a detailed survey map. The grid size in the plane is finest around the river, where the mesh size is approximately 20 m on average. The mesh size becomes larger with distance from the river, reaching approximately 100 m at the lateral boundaries of the model. The numerical model consists of 234 triangle pole elements.

The model is also divided vertically into four layers, as conceptualized in the previous section. However, the deepest Layer 4, which consists of alternating layers of coarse and fine sediments, is modeled only in the upper part (KP≥ 17.2), and the model bottom corresponds to the tertiary bedrock. On the other hand, the model in the lower part (KP< 17.2) is vertically restricted above the shallowest aquitard, instead of the tertiary bedrock. The restriction efficiently enables reasonable estimation of river seepage in such a regional model, because the estimation requires vertical flows of groundwater, not throughout the domain but only near the ground around the losing river. In most alluvial fans, the hydrogeologic basement suddenly declines in the downward direction, and uncertainty in modeling the deep zone might be too large to estimate river seepage. Thus, this study demonstrates a straightforward approach of assigning the constant boundary conditions on the shallowest aquitard, instead of no flow boundary conditions on the deep basement, such that vertical flows in the subsurface can be calculated with higher accuracy. The upper extent of the shallowest aquitard is assumed to be at the middle (KP 17.2) on the basis of previous drilling records (Sakata and Ikeda 2013b). The top of the aquitard and base rock (the model bottom) is also mapped according to these drilling records (the map is omitted in this paper). Consequently, the numerical model is composed of Layers 1, 2, and 3 on the aquitard (up to KP 17.2), and of Layers 2, 3, and 4 on the impermeable base rock (beyond KP 17.2).

Inflow boundary conditions are given in river cells, and the constant head is assigned from the measured river stage. Outflow boundary conditions are also assigned in model side cells and the bottom cells. The latter condition is a straightforward way to describe downward flow around the losing river. It should be noted that in most conventional models, no vertical flow boundary is assumed for bottom cells. The constant head values used here on the sides and bottom are given by linearly interpolating a WTE map from the VHG map. Constant head is also assigned on the downstream side (KP 17.2) of Layer 4. Thus, groundwater recharge to the deeper Layer 4 is estimated as a sum of discharge fluxes throughout the downstream side and the bottom. No flow boundary conditions are assigned on ground cells that are not river cells, because precipitation is small enough to be negligible for the drought period, as described above. Another reason is that evaporation rarely affects the deep water table, where depths exceed about 10 m in the fan, except around the river.

Spatial variability of horizontal hydraulic conductivity K was previously modeled on the basis of an undisturbed core analysis (Ito and Sakata 2009). The aquifer symbols G1, G2, and G3 in the previous work correspond to Layers 2, 3, and 4 in this paper. Figure 6 shows examples of longitudinal distributions of K at different depths in Layers 2, 3, and 4. K varies by over three orders of magnitude; lateral variation is relative to fining of grain size, and vertical variation is relative to reduction of open voids between gravel in the undisturbed cores. K in Layer 1 is assigned to be constant at the previous value (Huh et al. 2010b), due to limitation of field measurements. This study assumes that layer-scale anisotropy (vertical to horizontal conductivity ratio) is constant within, but may be different between each layer. The ratio is determined in sensitivity analysis as below. This study also assumed that permeability in the streambed was equal to that in the aquifer, that is, to the trend model of K at a depth of

zero. Specific storage, total porosity, and effective porosity values are assumed to be constant at 10^{-4} m^{-1}, 0.3, and 0.1, respectively, but these storage parameters are less sensitive than *K* in this steady flow simulation. Table 1 summarizes aquifer characteristics and hydraulic properties used in this simulation.

Model calibration

This study demonstrates model calibration by adjusting VHG map and layer-scale anisotropy to match observed and calculated heads in the monitoring wells. The initial VHG map is used to assign the constant head boundary on the bottom, but was constructed from limited piezometer nests and consequently includes uncertainty. The present study adjusts the VHG distribution from −0.04 to 0.04 in 0.02 increments. The adjusted values are provided individually in three sub-divided areas: (1) KP 14.0−16.8, (2) KP 16.8−17.4, and (3) KP 17.4−18.2 (Fig. 6). This study also assumes an additional aquifer parameter, layer-scale anisotropy, to realize the shallow water table under the constant head boundary conditions for the VHG peak. The fan deposits are generally composed of various facies. Anisotropy occurs as a result of such alternating layers of different permeability. Anisotropy in aquifers can be investigated *in situ*, for example by using multiple pumping tests (e.g., Weeks 1969). However, such *in situ* measurements of anisotropy are rarely performed in this fan. Layer-scale anisotropy for such a regional model might not be matched with that obtained from *in situ* measurements, except when a sufficient number of measurements are performed (a rare case in practice). Vertical anisotropy ratios (vertical / horizontal *K*) were assigned to each aquifer as unknown aquifer parameters (Anderson and Woessner 1992, pp. 69–70). This study simply inputs three cases of anisotropic ratio,1.0 (isotropy), 0.1, and 0.01 (dimensionless) in Layers 1 to 3, and determines individual values in terms of hydraulic head under a steady condition with the boundary conditions. Although only three patters

of anisotropy are prepared for this calibration, optimized model can provide sufficiently small values of error estimators.

Groundwater levels were calculated using an iteration process that assumes a correlation between groundwater heads and water exchange. First, groundwater levels were calculated under the initial boundary condition. The discrepancy between the specified river stage and calculated groundwater heads was used to calculate inflow and outflow through each river cell. Next, the water fluxes in the river cells were input as the discharge and recharge of specified fluxes. That is, they were used as Dirichlet conditions, under which groundwater levels were then recalculated. As before, water fluxes in each river cell were obtained from calculated groundwater heads. The process was iterated until convergence of the heads was achieved (at most 0.01 m in any cell). This study applies mean error (ME), root mean square error (RMSE), and normalized RMSE (RSMN, calculated by dividing RMSE by the discrepancy between maximum and minimum observed heads; 59.1 m here) at 43 observed heads for model optimization. The error estimators are calculated using the following equations:

$$\mathrm{ME} = \sum_{j=1}^{N} \left(H^{\mathrm{cal}}{}_j - H^{\mathrm{obs}}{}_j \right) \Big/ N \tag{1a}$$

$$\mathrm{RMSE} = \sqrt{\sum_{j=1}^{N} \left(H^{\mathrm{cal}}{}_j - H^{\mathrm{obs}}{}_j \right)^2 \Big/ N} \tag{1b}$$

$$R\mathrm{MSN} = \mathrm{RMSE} \big/ \left(H^{\mathrm{obs}}{}_{\mathrm{max}} - H^{\mathrm{obs}}{}_{\mathrm{min}} \right) \tag{1c}$$

Here, H is the groundwater level, subscript j is the code number of the observation well, N is the number of monitoring wells (43 in this study), and the superscripts cal and obs stand for calculated and observed water-level values, respectively. $H^{\mathrm{obs}}{}_{\mathrm{max}}$ and $H^{\mathrm{obs}}{}_{\mathrm{min}}$ are the maximum and minimum of measured head values, respectively. The mean error

is a measure of the overall bias of the predictions. The RMSE is usually used as the best error estimator if errors are normally distributed, and the errors are only a small part of the overall model response when the RMSN is small (Anderson and Woessner 1992, p. 241). In this study, a model is acceptable when RMSE values are less than 0.1 (10 %) for a regional-scale model.

RESULTS AND DISCUSSION

Hydraulic heads

Figure 6 shows the relation between calculated and observed heads in the initial (a) and calibrated (b) models. Even in the initial model, most calculated heads appear to be only slightly different from the observed heads. However, the calculated heads in shallow wells are several meters lower than the observed heads, particularly around the VHG peak. In contrast, the optimized model calculates reasonable heads for all monitoring wells. The error estimators, ME, RMSE, and RMSN, were only 0.29 m, 0.74 m, and 1.0%, respectively. The adjusted VHG values were +0.01 in Section (1), 0.00 in section (2), and −0.04 in section (3). The anisotropy ratio was also assumed to be constant at 0.1 in Layers 1, 2, and 3, and at 0.01 in Layer 4. The small ratio in Layer 4 is qualitatively interpreted as being due to more frequent changes of gravel, sand, and clay in the various depositional environments than are present in Layers 2 and 3 in the fan developments. One might consider the anisotropy values to be oversimplified, and that error estimators could be smaller if the parameters are adjusted in more detail. However, the small RMSN value indicates that the optimized model sufficiently realized the three-dimensional flow of groundwater in the fan.

River seepage

Figure 9a shows calculated longitudinal variations of specific water exchange q (m^3/s per km). Negative and positive values indicate surface water loss and gain, respectively. Figure 9a showed that the specific exchange q largely fluctuated in the upper part from KP 18.5. This is because the river cells are relatively close to the east and west boundaries with constant head conditions. The specific exchange is relatively large and positive (negative) when the river channel is adjacent to the east (west) side, where the constant head is generally larger (smaller) than the river stage. In the middle, between KP 18.5 and KP 15, the specific exchanges are generally negative, indicating the losing reach of this river. The magnitude was less than 0.4 m^3/s per km, and the range of q is typical when compared with other alluvial fans in Japan (Sasaki 1974). The positive q around KP 16.4 is attributable to the large groundsills, where the river stages are suddenly lower relative to the water table. Other groundsills (KP 15.2, 15.9, and 17.4) also cause fluctuation in q within each local area. Finally, in the lower part from KP 15 the specific exchanges were nearly zero, indicating no interaction between surface water and groundwater.

Figure 9b also shows the surface water budget dQ (flow discharge change) in relation to only groundwater—that is, excluding other components such as inflow from the tributaries. The surface water budget dQ is calculated by summing products of water exchange values q at a constant distance (0.2 km) from the uppermost section. The change in dQ looks smoother than q, especially around the groundsills, as a result of the summation of dQ. The surface water budget decreases downstream in most of the fan, except between KP 20.6 and 21.4. The water gain in the uppermost section is balanced with the water loss, and the net water budget in the upper section is -0.1 m^3/s. In the middle section, the budget decreases linearly and the net water loss is calculated to be 1.0 m^3/s. The negative slope becomes gentle around KP 15, and the water budget

appears to be almost neutral in the lower section from KP 15. Thus, the total river seepage is calculated to be 1.1 m^3/s, but the water gain is not calculated in this model.

Figure 9b shows the average of four results from a previous synoptic survey between KP 11 (gauging station R1) and KP 18.5 (the confluence with the Yamahana River), as shown in Fig. 5 of Sakata and Ikeda (2012). These four results were all obtained at the low river stages, which were several tens of centimeters different from the drought period for analysis. However, Fig. 9b shows only the average for comparison because individual results fluctuated randomly due to measurement errors in different flow conditions. The survey results indicated water loss upstream from KP 15.2 (one of the surveying transects), and conversely water gain downstream. The average results are clearly consistent with results calculated for the upstream area (from approximately KP 15). Considering the agreement between the simulation and survey results, this study determined river seepage to be approximately 1.0 m^3/s between KP 15 and KP 18.5. The result for the losing section is probably more accurate than the previous estimates for the section between KP 15.5 and 17.0.

The simulation results also indicate that a change from water loss to gain occurs around at KP 13. However, there is a large discrepancy between the simulation results for water gain in the lower fan and the synoptic survey results. The simulated water gain was only 0.1 m^3/s between KP 11 and KP 13, and the synoptic survey revealed that the total water gain was approximately 0.5 m^3/s downstream from KP 15.2. One reason for the difference may be geologic simplification; hydraulic conductivity K is assumed to be a continuously decreasing function, as shown in Fig. 7. In actuality, alluvial deposits in the lower fan are similar to meandering river or delta deposits, where thin finer layers are much more frequently intersected within the gravel deposits than in the upper fan, as shown in Fig. 2. However, such complicated sedimentary textures in the lower fan were

not considered in this model, due to insufficient geologic data. A sudden reduction of permeability in the distal region might prevent lateral groundwater flow, and then shallow groundwater flow would alternately discharge to the river, as the field measurements indicated. The following discussion interprets the outflow fluxes of groundwater on lower sides as an estimation error in this model, and alternately as water gain in the river.

Groundwater budget

Table 2 summarizes calculated boundary fluxes of groundwater in the modeled area. Here, the fan is longitudinally divided into three areas: upper (KP 18.5 to KP 21), middle (KP 15 to KP 18.5), and lower (KP 11 to KP 15) sections. The lower (recalculated) section shown in the table is obtained under the assumption that lateral fluxes to the north and east sides are changed to a discharge along the river boundary. Each component is rounded to one decimal place in meters per second, and components less than 0.1 m/s are treated as zero. Figure 10 also shows schematic groundwater budgets during the drought period in the Toyohira River alluvial fan. Groundwater fluxes on the surface boundary (precipitation P and evaporation E) were assumed to be zero during the drought period. Total P in the month before the observation dates was 78.5 mm, and total E in the period was also estimated to be 69 mm by using the Thornthwaite (1948) method. Thus, $P-E$ is only −10 mm/month, and the value is less than 0.1 m^3/s over the model area (16 km^2). The groundwater budgets are entirely balanced in the upper section; the sum of lateral groundwater fluxes through the east and west boundaries is equal to the water gain in the river to within the order of magnitude 0.1 m/s. This means that groundwater flows from the high relief serve surface water flows, rather than directly contributing to the reservoirs.

In the middle section, river seepage is calculated at 1 m^3/s (Fig. 9). Inflow groundwater flux GW^{in} from the east Pleistocene fan is 0.1 m^3/s larger than outflow flux GW^{out} to the west Holocene fan. Thus, the groundwater recharge in the middle section is estimated at 1.1 m^3/s. The vertical discharge to the bottom boundaries (Layer 4) is 0.5 m^3/s, and the residual groundwater (0.6 m^3/s) flowed downstream to the lower section through Layers 2 and 3. Additional vertical fluxes to the bottom are 0.1 m^3/s in the lower section. Therefore, the total discharge fluxes to the deep aquifer were calculated at 0.6 m^3/s, and the value almost matches the total pumping rate in the Chuo ward of Sapporo in 2008 (Sapporo City 2014). Considering that most water wells are installed in deeper aquifers, river seepage serves as the main source of recharge in the alluvial fan, especially during drought periods.

In the lower section, this simulation calculated a water gain of 0.1 m^3/s, a value that is probably unrealistic given the synoptic survey results. Water gain has significance not only for the surface water budget, but also for ecological environments such as salmon spawning grounds. If K was one order of magnitude smaller than in the model that includes fining grain sizes, the lateral fluxes to the south and east would be zero to on the order of 0.1 m^3/s. Thus, the lower (recalculated) condition in Table 2 summarizes the case where the calculated lateral fluxes on the side boundaries are assumed to be zero and the discharge to the river boundary is 0.5 m^3/s. This discharge value is equal to the water gain calculated as the average of the previous synoptic discharge in Fig. 9.

This simulation determined a river seepage of 1 m^3/s in the middle section between KP 15 and KP 18.5. One half of the infiltrated water flowed downstream in the shallower Layers 2 and 3, and returned to the river in the lower fan. Another half was discharged to the deep aquifer IV, contributing to water intake in the city. Interestingly,

the groundwater discharges in the shallow and deep layers are in agreement despite a large difference in permeability between the aquifers. Overall, the results strongly support the importance of river seepage for both the hydrologic cycle in the alluvial fan and human and natural consumption. In particular, considering the agreement with water intake and recharge in the deep aquifer, Sapporo is threatened with groundwater vulnerability during drought periods, which might become more frequent due to sharp reduction of precipitation under climate change (Hu *et al*. 2010b).

Model limitations

This modeling approach includes several uncertainties and limitations in terms of space and time. This numerical groundwater model is composed of a limited number of aquifers in an area restricted to the shallow aquitard in the fan. Thus, the model provides constrained realizations of groundwater flow in the subsurface area. Additionally, groundwater flow largely depends on boundary conditions at the bottom, although determination of the conditions includes uncertainty in relation to head data. The simulation assumed that the river seepage was almost constant during drought periods. One might require river seepage to be estimated throughout one hydrologic cycle, including focused recharge by snow melting and precipitation events. Water loss transiently varies during shorter events such as floods, generally increasing with water discharge (Vasiliev 1987, Frei *et al*. 2009). The regional-scale model is not suitable for such diverse discharge conditions for limited head data in the deep aquifer. However, it is commonly the case that head data for model calibration are also insufficient in space and time to describe overall systems in an alluvial fan. As in this study, a conditioning approach is typically utilized to estimate groundwater flow in a local area and thereby to effectively provide plausible estimates of river seepage in a specified area.

CONCLUSIONS

This study performed a groundwater simulation of river seepage in the Toyohira river alluvial fan through constant head boundary conditions on the model bottom. The VHG for the boundary was assigned on the basis of a VHG map manually constructed from several piezometer nests. Model calibration was performed by adjusting the initial map and by assuming layer-scale anisotropy of permeability. An optimized model provided almost the same hydraulic heads as the observations. As a result, the simulated river seepage was in reasonable agreement with the results of a previous synoptic survey, and the leakage was determined to be approximately 1 m^3/s between KP 15 and KP 18.5. Half of the recharge flowed downstream through the shallow aquifer and returned to the river in the lower fan. Half of the net loss was discharged from the bottom boundary to the deeper aquifer, where most water wells in Sapporo are installed. However, the simulation failed to estimate water gain in the lower fan, probably due to uncertainty in sporadic intercalation of fine sediments in this model. Despite being constrained to steady flow in the shallow zone, this conditioned VHG modeling approach can contribute to efficient estimations of river seepage on regional scales, particularly given that losing and gaining reaches have rarely been identified in advance. It is also expected that the proposed modeling approach will be applicable to other problems regarding shallow groundwater flows within regional flow systems, such as basin-scale land subsidence due to withdrawal from a deep aquifer. Also, recent developments in computing have enabled the handling of much more complicated 3D models in various conditioning patterns than in this study. Thus, in future research, we plan to incorporate models with various vertical scales: (1) regional scale to the basement; (2) intermediate scale to the shallowest aquitard (the same in this study); and (3) local scale within Layer 2 around river channels. In such an advanced approach, the boundary conditions in each model would be simultaneously supported by the results in

the other scale models, such that the groundwater system could be realized in a more quantitative manner for scientific and engineering purposes.

Acknowledgements The authors acknowledge the Hokkaido Regional Development Bureau and Geological Survey of Hokkaido for permission to use monitoring wells and technical reports. We express their sincere gratitude with co-editor, Dr. Demetris Koutsoyiannis, and assistant editor, Dr. James Ward, for their suggestions and encouragement on this issue. We also greatly thank Dr. Amartya Kumar Bhattacharya and two anonymous reviewers, for providing insightful comments to improve this paper. Technical support for this numerical study was received with gratitude from our colleagues, Sayuri Watanabe, Yoko Yamamoto, and Asaki Yoshida.

References

Anderson, M.P. and Woessner, W.W., 1992. *Applied Groundwater Modeling Simulation of Flow and Advective Transport*. London: Academic press.

Blainey, J.B. and Pelletier, D., 2008. Infiltration on alluvial fans in arid environments: Influence of fan morphology. *Journal of Geophysical Research*, 113, F03008.

Bull, W.B., 1964. Geomorphology of segmented alluvial fans in western Fresno County, California. *U.S. Geological. Survey Prof. Paper*, 352–E, pp. 89–129.

Calver, A., 2002. Riverbed permeabilities: Information from pooled data. *Ground Water*, 39(4), 546–553.

Chen, C.H., Wang, C.H., Hsu, Y.J., Yu, S.B. and Kuo, L.C., 2010. Correlation between groundwater level and altitude variations in land subsidence area of the Choshuichi Alluvial Fan, Taiwan. *Engineering Geology*, 115, 122–131.

Fetter, C.W., 2001 *Applied hydrogeology*. 4th ed. Upper Saddle River, New Jersey, USA: Prentice-Hall.

Fleckenstein, J.H., Niswonger, R.G. and Fogg, G.E., 2006. River-aquifer interactions, geologic heterogeneity, and low-flow management. *Groundwater*, 44(6), 837–852.

Frei, S., Fleckenstein, J.H., Kollet, S.J. and Maxwell, R.M., 2009. Patterns and dynamics of river–aquifer exchange with variably-saturated flow using a fully-coupled model. *Journal of Hydrology*, 375, 383–393.

Fugazza, M., Gallati, M., Moisello, U. and Natale, U., 1983. Integration of surface water with groundwater resources aided by numerical modeling. *Hydrological Sciences Journal*, 28(1), 155–168.

Gupta, A.D. and Onta, P.R., 1997. Sustainable groundwater resources development. *Hydrological Sciences Journal*, 42(4), 565–582.

Healy, R.W., 2010. *Estimating Groundwater Recharge*. Cambridge: Cambridge University Press.

Hu, S.G., Kobayashi, T., Okuda, E., Oishi, A., Saito, M., Kayaki, T. and Miyazaki, S., 2010a. Alluvial fans-importance and relevance: a review of studies by Research group on Hy-dro-environments around alluvial fans in Japan. *In*: M. Taniguchi, and

I.P. Holman, eds. *Groundwater Response to Changing Climate*, AK Leiden, Netherlands: CRC Press, 131–139.

Hu, S.G., Miyajima, S., Nagaoka, D., Koizumi, K. and Mukai, K., 2010b. Study on the relation between groundwater and surface water in Toyohira-gawa alluvial fan, Hokkaido, Japan. *In*: M. Taniguchi, and I.P. Holman, eds. *Groundwater Response to Changing Climate*, AK Leiden, Netherlands: CRC Press, 141–158.

Houston, J., 2002. Groundwater recharge through an alluvial fan in the Atacama Desert, northern Chile: mechanisms, magnitudes and causes. *Hydrological Processes*, 16, 3019–3035.

Ito, K. and Sakata, Y., 2009. Groundwater modeling study in the Toyohira River alluvial fan I: spatial variability of hydraulic conductivity in alluvial gravel deposits. *Autumn Proceedings of the Japan Society of groundwater hydrology, 16 October 2009, Sapporo, Japan*, 52–55 (in Japanese).

Jang, C.S. and Liu, C.W., 2005. Contamination potential of nitrogen compounds in the heterogeneous aquifers of the Choushui River alluvial fan, Taiwan. *Journal of Contaminant Hydrology*, 79, 135–155.

Japan Meteorological Agency, 2012. National Climate Data and Information Archive. Available from: http://www.data.jma.go.jp/obd/stats/etrn/index.php [Accessed 4 December 2012].

Maruyama, T., Yoshida, M., Takase, K., Takimoto, H., Ishikawa, S. and Nagasaka, S., 2013. Long-term assessment of nitrogen pollution load potential for groundwater by mass balance analysis in the Tedori River alluvial fan area, Japan. *Journal of Water Resource and Protection*, 5, 171–182. Nobi, N. and Gupta, A.D., 1997. Simulation of regional flow and salinity intrusion in an integrated stream-aquifer system in coastal region: southwest region of Bangladesh. *Groundwater*, 35, 786–796.

Okayama University, 1994. GEL Download page. Available from: http://gw.civil.okayama-u.ac.jp/gel_home/download/index.html [Accessed 14 March 2012].

Ono, Y., 1990. Alluvial fans in Japan and South Korea. *In*: A.H., Rachocki and M., Church, eds. *Alluvial fans: a field approach*. Baffins Lane, Chichester, West Sussex, UK: John Wiley and Sons, 91–108.

Pisinaras, V., Petalas, C., Tsihrintzis, V.A. and Zagana, E., 2007. A groundwater flow model for water resources management in the Ismarida plain, North Greece. *Environmental Modeling and Assessment*, 12(2), 75–89.

Pucci, A.A. and Pope, D.A., 1995. Simulated effects of development on regional groundwater/surface-water interactions in the northern Coastal Plain of New Jersey. *Journal of Hydrology*, 167, 241–262.

Rodríguez, L.B., Cello, P.A. and Vionnet, C.A., 2006. Modeling stream-aquifer interactions in a shallow aquifer, Choele Choel Island, Patagonia, Argentina. *Hydrogeology Journal*, 14, 591–602.

Saito, K., 1998. *Alluvial fans in Japan*. Tokyo, Japan: Kokon-Shoin (in Japanese).

Sakata, Y. and Ikeda, R., 2012. Quantification of longitudinal river discharge and leakage in an alluvial fan by synoptic survey using handheld ADV. *Journal of Japan Society of Hydrology and Water Resources*, 25, 89–102 (in Japanese).

Sakata, Y. and Ikeda, R., 2013a. Regional mapping of vertical hydraulic gradient using uncertain well data: a case study of the Toyohira River alluvial fan, Japan. *Journal of Water Resource and Protection*, 5, 823–834.

Sakata, Y. and Ikeda, R., 2013b. Depth dependence and exponential models of permeability in alluvial-fan gravel deposits. *Hydrogeology Journal*, 21, 773–786.

Sapporo City, 2014. Annual Reports and Environmental Data. Available from:

http://www.city.sapporo.jp/kankyo/kankyo_data/h20pdf.html [Accessed 13 June 2013].
Sasaki, T., 1974. On the influent seepage from rivers on alluvial fans. *Hydrology*, 6, 35–38 (in Japanese).
Sebok, E., Duque, C., Engesgaard, P. and Boegh, E., 2014. Spatial variability in streambed hydraulic conductivity of contrasting stream morphologies: channel bend and straight channel, *Hydrological Processes*, published online, available from: http://onlinelibrary.wiley.com/doi/10.1002/hyp.10170/pdf [Accessed 10 February 2014].
Sophocleous, M., 2002. Interactions between groundwater and surface water: the state of the science. *Hydrogeology Journal*, 10, 52–67.
Thornthwaite, C.W., 1948. An approach toward a rational classification of climate. *Geographical Review*, 38, 55–94.
Toleman, C.F., 1937. *Groundwater*. New York, USA: McGraw-Hill.
Vasiliev, O.F., 1987. System modelling of the interaction between surface and ground waters in problems of hydrology. *Hydrological Sciences Journal*, 32(3), 297–311.
Week, E.P., 1969. Determining the ratio of horizontal to vertical permeability by aquifer-test analysis. *Water Resources Research*, 5(1), 196–214.
Weight,W.D., 2008. *Hydrogeology Field manual*, 2nd ed. New York, USA: McGraw-Hill.

Table 1. Summary table of aquifer characteristics and input properties. *K* denotes horizontal hydraulic conductivity, and calibrated anisotropy is layer-scale vertical to horizontal conductivity ratio as a result of sensitivity analysis. Other storage parameters are described in texts.

Components	Layer			
	I	II	III	IV
Lithology	Sand, silt and peat	Sandy gravel and cobble		Silt, sand and gravel
Typical Thickness (m)	–10 (KP13)	20– 30	20– 40	–70 (KP17.2)
K (m/s)	2×10^{-5}	Decreasing trend assigned (Fig. 5)		
Calibrated anisotropy (–)		0.1		0.01

Table 2. Calculated groundwater fluxes (in and out) in the numerical model. Positive and negative values denote recharge (inflow) and discharge (outflow), respectively. The classification of upper, middle, and lower sections is described in the text. The lower section shows the original (left) and interpreted (right) results, in which all discharges are integrated to water gain in the river. The "Total" column shows the sum of fluxes in the upper, middle, and lower (recalculated) sections for each row.

Boundary		Upper Section	Middle section	Lower section		Total
				original	recalculated	
River		0.1	1.0	0	–0.5	0.6
Sides	East	0.1	0.2	–0.2	0	0.3
	West	–0.2	–0.1	–0.1	0	–0.3
	South	0	-	-	-	0
	North	-	-	–0.2	0	0
Bottom		0	–0.5	–0.1	–0.1	–0.6
Surface		0	0	0	0	0

in m^3/s

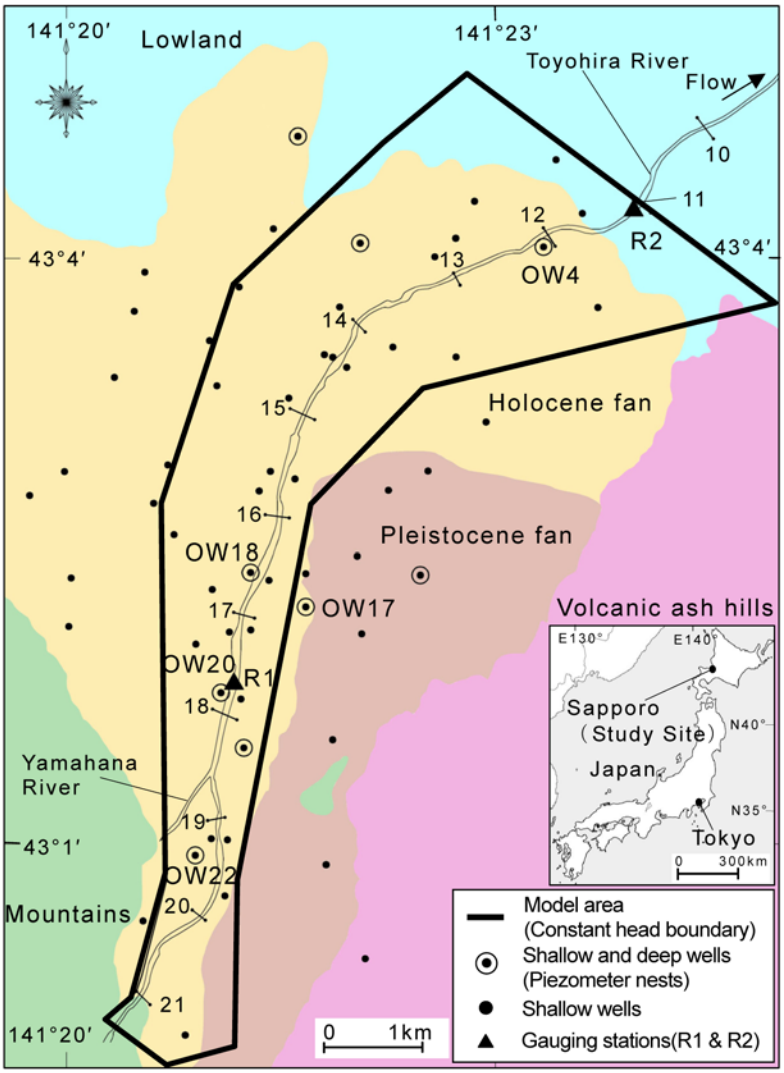

Fig. 1 Location maps and topographic features of the study area, the Toyohira River alluvial fan. The black lines across the river indicate the distance in kilometers, denoted as KP throughout the text. Gauging stations R1 and R2 are located on the river at KP 17.8 and KP 11, respectively. Sky blue, yellow, brown, purple, and green denote topographic features: the low land, Holocene fan, Pleistocene fan, volcanic ash hills, and mountains, respectively.

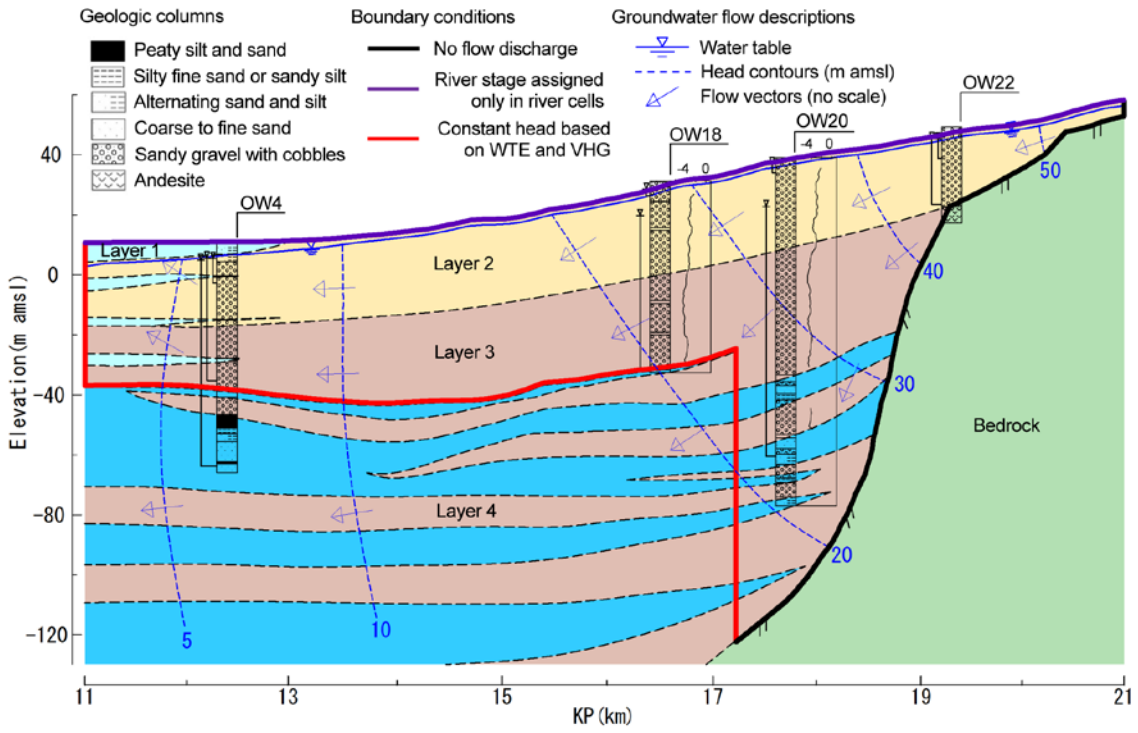

Fig. 2 Geologic cross section of the fan subsurface. Inverted open triangles denote piezometric heads in the drought period for analysis. Colors except dark blue (deeper fine deposits in Layer 4) correspond to those in Figure 1. Profiles of the common logarithm of K at OW18 and 20 are obtained from an undisturbed core analysis in Sakata and Ikeda (2013b).

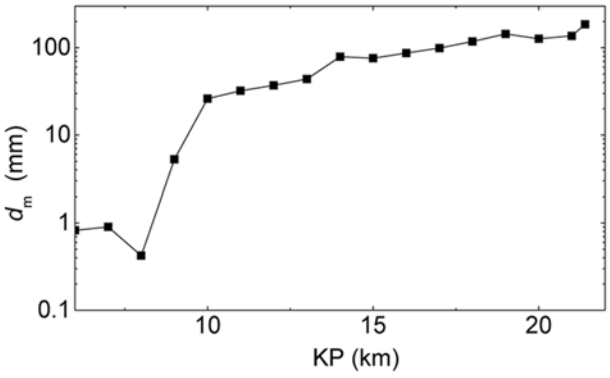

Fig. 3 A longitudinal distribution of the median grain size of the bed material in each kilometer (KP) along the Toyohira River.

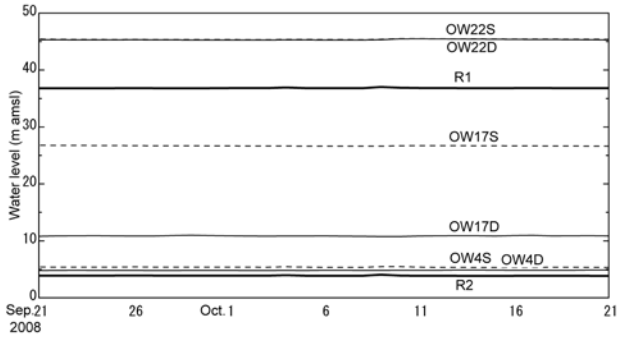

Fig. 4 Observed variations in water levels at gauging stations and observations wells. The locations of gauging stations and monitoring wells are shown in Fig. 1.

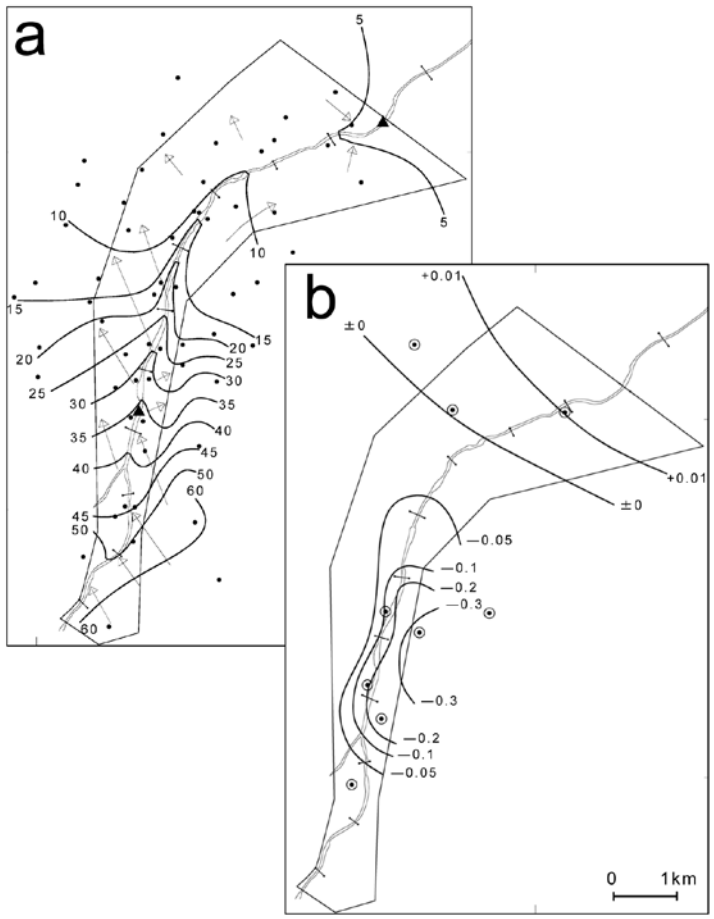

Fig. 5 Contour maps of (a) WTE and (b) VHG during a drought period for analysis. The monitoring wells correspond with those in Fig. 1. WTE contours are illustrated per 5 m amsl. Negative (positive) values of VHG indicate downward (upward) hydraulic gradient (dimensionless).

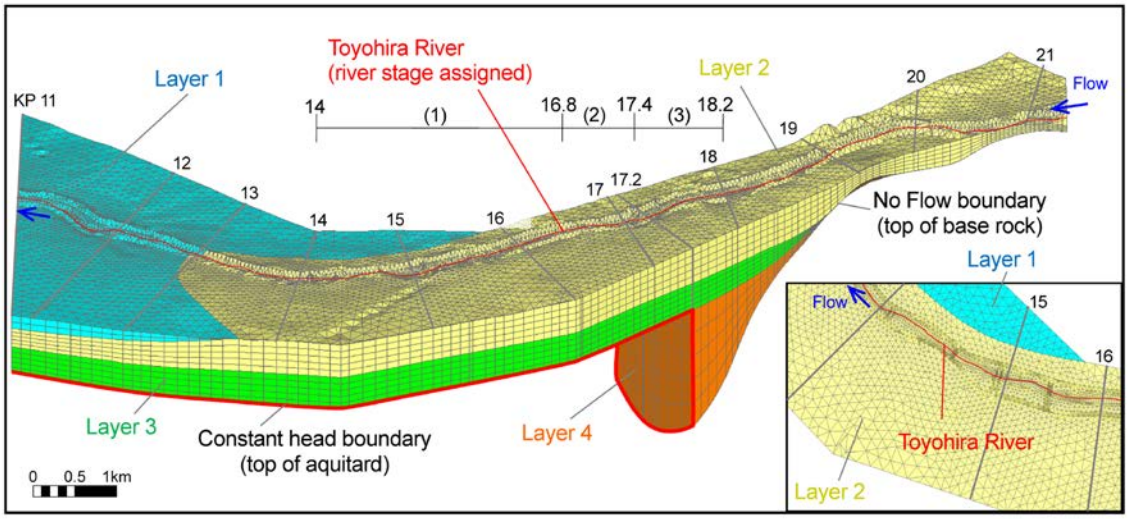

Fig. 6 Numerical groundwater flow model in the Toyohira River alluvial fan.

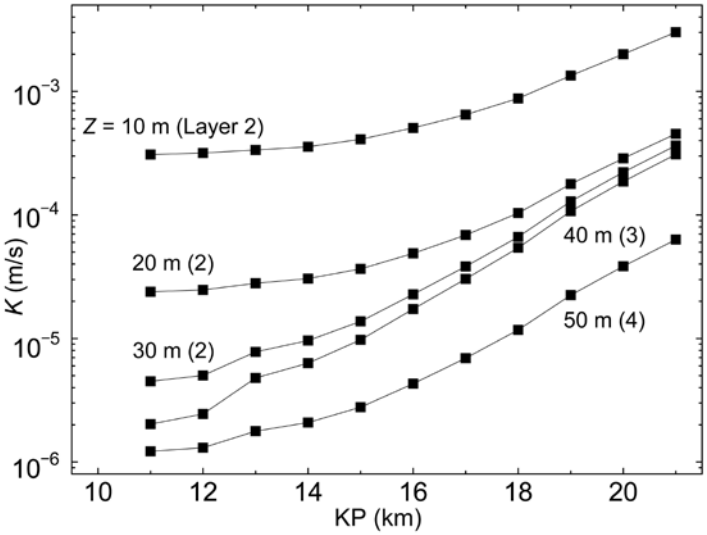

Fig. 7 Longitudinal distributions of hydraulic conductivity at different depths Z per ten meters with layer numbers (Layers 2, 3, and 4).

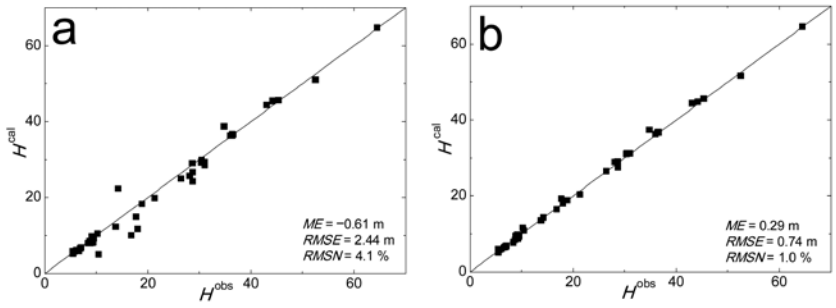

Fig. 8 Relations between simulated heads H^{cal} and observed heads H^{obs} at 43 monitoring wells using (a) the initial model and (b) the optimized model.

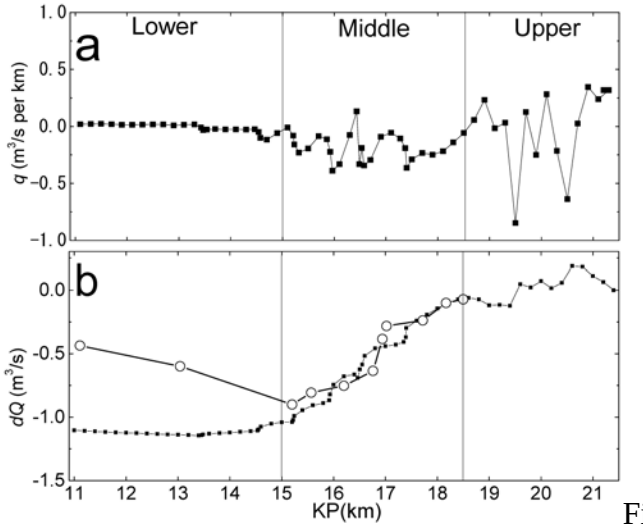

Fig. 9 Simulated results of (a) specific water loss and (b) surface water budget. Negative and positive values indicate water loss and gain, respectively. Open circles in (b) are average values from previous synoptic discharge survey results.

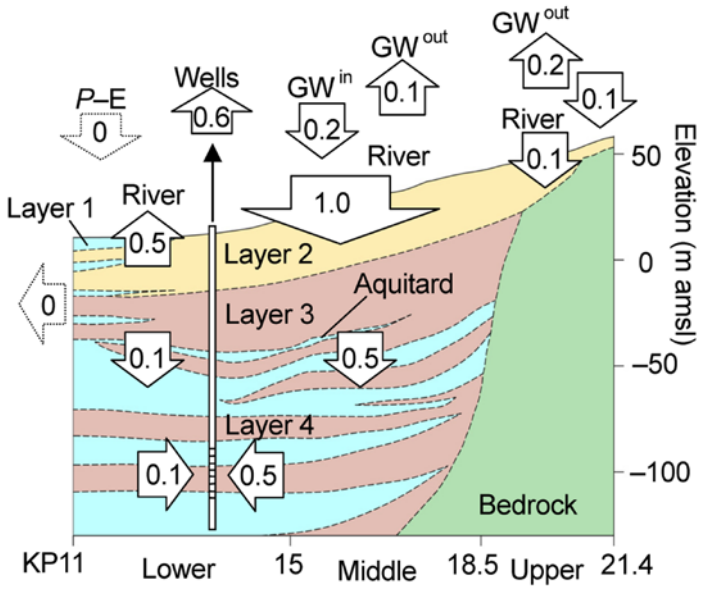

Fig. 10 Schematic subsurface groundwater budgets in the Toyohira River alluvial fan, obtained by modifying the longitudinal and vertical scales in Fig. 2. The values in arrows are rounded to one order of magnitude in cubic meters per second. GW^{in} and GW^{out} denote groundwater recharge from the east side and discharge to the west side, respectively.